(A jeopardy proposal to Jefferson Lab PAC29)

Polarization transfer in Wide Angle Compton Scattering

P. Bosted, J. P. Chen, E. Chudakov, C. DeJager, R. Ent, R. Feuerbach, J. Gomez, O. Hansen, D. W. Higinbotham, M. Jones, J. LeRose, R. Michaels, S. Nanda, B. Reitz, A. Saha, S. A. Wood, B. Wojtsekhowski (spokesperson and contact person)
Thomas Jefferson National Accelerator Facility, Newport News, VA 23606

A. Danagoulian, A.M. Nathan (spokesperson), M. Roedelbronn
University of Illinois, Champaign-Urbana, IL 61801

C. Glashausser, R. Gilman (spokesperson), X. Jiang, E. Kuchina, G. Kumbartzki, R. Ransome, J. Yuan
Rutgers, The State University of New Jersey, Piscataway, NJ 08854

V. Kubarovsky[†], J. Napolitano, P. Stoler
Rensselaer Polytechnic Institute, Troy, NY 12180-3590

K. Egiyan, V. Mamyan, A. Shahinyan, H. Voskanyan
Yerevan Physics Institute, Yerevan, Armenia

F. Cusanno, F. Garibaldi, S. Frullani, G. M. Urciuoli, M. Iodice
INFN, Rome, Italy

R. De Leo, L. La Gamba
INFN, Bari, Italy

D. Nikolenko, I. Rachek, Yu. Shestakov
Budker Institute, Novosibirsk, Russia

F. Butaru, Z.-E. Meziani, P. Solvignon, H. Yao
Temple University, Philadelphia, PA 19122

J. Annand, A. Borissov, D. Ireland, D. Protopopescu, G. Rosner, D. Watts
University of Glasgow, Glasgow, Scotland

P. Markowitz
Florida International University, Miami, FL 33199

G. Chang, J. J. Kelly
University of Maryland, College Park, MD 20292

M. Khandaker, V. Punjabi
Norfolk State University, Norfolk, VA 23504

B. Crowe, B. Vlahovic
North Carolina Central University, Durham, NC 03824

J. M. Laget, F. Sabatie
CEA Saclay, Gif-sur-Yvette, France

E. Piasetzky, G. Ron
Tel Aviv University, Israel

C. Perdrisat, L. Pentchev
College of William and Mary, Williamsburg, VA 23185

C. Hyde-Wright, A. Radyushkin
Old Dominion University

P. Kroll
Fachbereich Physik, Universitat Wuppertal, Germany

V. Nelyubin
St-Petersburg Institute Nuclear Physics, Russia

A. Vasiliev
IHEP, Protvino, Russia

D. Margaziotis
California State University Los Angeles, Los Angeles, CA 90032

P. Bertin
University Blaise Pascal/IN2P3, France

R. Lindgren, B. E. Norum, K. Wang
University of Virginia, Charlottesville, VA 22901
† on leave from *IHEP, Protvino, Russia*

December 5, 2005

Abstract

An experiment is proposed to measure the components of the recoil proton polarization in Real Compton Scattering (RCS) with longitudinally polarized incident photons. Measurements are proposed at s= 9 (GeV/c)^2 for three values of the θ_p^{cm} = 70°, 90°, and 110°.

The recent JLab RCS experiment, E99-114, demonstrated the feasibility of the experimental technique and produced a remarkable result. Namely, at s= 7 (GeV/c)^2 and θ_p^{cm} = 120°, the longitudinal polarization is in agreement with the handbag description of the process in which the photons interact with a single quark, but is completely inconsistent with a pQCD mechanism which involves three active quarks mediated by two hard gluon exchanges. It is essential to have additional measurements over a broader kinematic range for complete experimental verification of the handbag mechanism. Besides testing the reaction mechanism, the measurements will also allow access to the axial and tensor form factors of the proton, R_A and R_T, respectively, which are moments of particular Generalized Parton Distributions.

The experiment utilizes an untagged bremsstrahlung photon beam and the standard cryogenic target. The scattered photon is detected in the BigCal photon spectrometer, recentrly constructed by the GEP-III collaboration. The coincident recoil proton is detected in the Hall A magnetic spectrometer HRS-L or Hall C magnetic spectrometer HMS, and its polarization components are measured in the existing Focal Plane Polarimeters. With 408 hours of beam time in Hall A and 56 hours of beam time in Hall C, each of the three polarization observables, K_{LL}, K_{LT}, and P_N, will be measured to a statistical accuracy of ± 0.1 at each kinematic point.

Such a measurement would significantly increase our experimental confidence in the handbag reaction mechanism which is expected to play a major role in exclusive reactions in the JLab energy range.

1 Introduction

Compton scattering in the hard scattering limit is a potentially powerful probe of the short-distance structure of the nucleon. It is a natural complement to other exclusive reactions, such as high Q^2 elastic electron scattering and high-energy meson photoproduction, where the common feature is a hard energy scale. For Real Compton Scattering (RCS), the hard scale is achieved when s, $-t$, and $-u$ are all large compared to the proton mass, or equivalently, when the transverse momentum transfer $p_\perp$ is large. Under such conditions one expects the transition amplitude to factorize into the convolution of a perturbative hard scattering amplitude, which involves the coupling of the external photons to the active quarks, with an overlap of initial and final soft (nonperturbative) wave functions, which describes the coupling of the active quarks to the proton. Schematically this can be written

$$T_{if}(s,t) \;\; = \;\; \Psi_f \otimes K(s,t) \otimes \Psi_i \,, \tag{1}$$

where $K(s,t)$ is the perturbative hard scattering amplitude, and the Ψ's are the soft wave functions. Different factorization schemes have been applied to RCS in recent years and these can be distinguished by the number of active constituents participating in the hard scattering subprocess. The pertubative QCD (pQCD) mechanism [1, 2, 3, 4] involves three active constituents, while the handbag mechanism [5, 6, 7] involves only one. In any given kinematic regime, both mechanisms will contribute, in principle, to the scattering amplitude. At "sufficiently high" energy, the pQCD mechanism is expected to dominate, but it is not known how high is sufficiently high or the manner in which the transition to the purely pQCD mechanism emerges. At sufficiently low energy (e.g., in the resonance region), RCS and other exclusive reactions are dominated by purely soft physics, and the amplitude does not factorize into hard and soft processes. At high energy but small $-t$ or $-u$, soft physics also dominates through Regge exchanges [8]. The nature of the transition from purely soft to the factorization regime is also not well known.

Quite aside from the reaction mechanism, it is of interest to ask what RCS can teach us about the nonperturbative structure of the proton and to relate it to that revealed in other reactions. There has been much theoretical progress in recent years in providing a unified description of inclusive and exclusive reactions in the hard scattering regime [5, 6, 7]. This is based on the concept of Generalized Parton Distributions (GPD's), which are superstructure of the nucleon from which can be derived the normal parton distribution functions (PDF's), elastic electron scattering form factors, and new form factors accessible only through Compton scattering.

With this backdrop, experiment E99-114 [9] was undertaken to study the RCS reaction. The primary focus was the measurement of precise spin-averaged cross sections over the kinematic regime of $5 \leq s \leq 11$ $(\mathrm{GeV}/c)^2$ and $1.5 \leq -t \leq 6.5$ $(\mathrm{GeV}/c)^2$. In addition, a measurement was made at a single kinematic point of the polarization transfer to the recoil proton using longitudinally polarized incident photons. The latter measurement has produced a remarkable result [10], which is shown in Fig. 1 and which will be discussed in

more detail in the next section of this proposal. Namely, the longitudinal polarization transfer is consistent with the handbag prediction and completely inconsistent with predictions based on pQCD. This gives very strong credence to the notion that the photons interact with a single quark. Indeed, the longitudinal polarization is nearly as large as that expected for scattering from a free quark. However, we emphasize that this is a measurement at a *single kinematic point*, and it is essential to verify the result with measurements over a broader kinematic range.

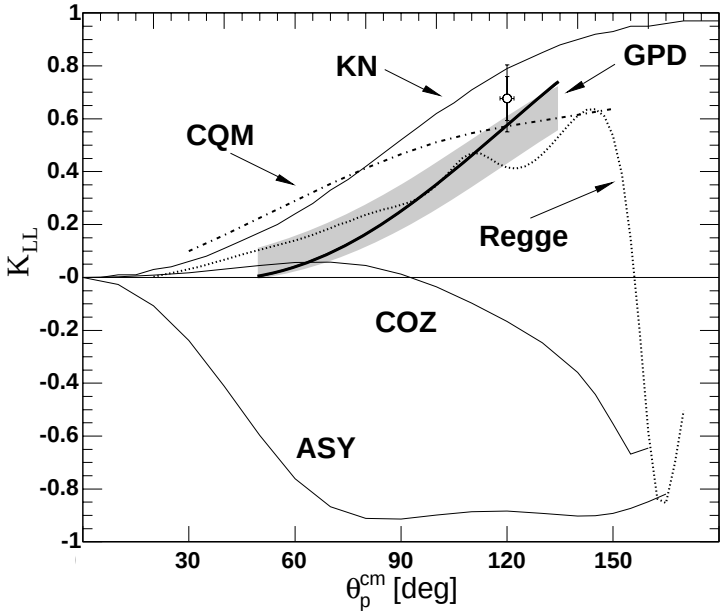

Figure 1: Longitudinal polarization transfer in the RCS process at an incident energy of 3.23 GeV [10]. The labels on the curves are KN for the asymmetry in the hard subprocess; GPD, shown as a gray band, for the handbag approach using GPD's [11]; CQM for the handbag approach using constituent quarks [12]; Regge for a Regge exchange mechanism [13]; and COZ and ASY for pQCD calculations [4] using the asymptotic (ASY) or Chernyak-Ogloblin-Zhitnitsky (COZ) distribution amplitudes.

We therefore propose new measurements of polarization observables in Compton scattering at an incident energy of 4.3 GeV, or s=9 $(\mathrm{GeV/c})^2$ at three different scattering angles. The proposal is organized as follows. In Section 2 we present our physics motivation and summarize the physics goals of the proposed experiment. In Section 3 we describe the experimental approach and both the standard and the specialized equipment. In subsequent sections, we present our proposed measurements (Sec. 4), our expected results and beam time request (Sec. 5), and the technical considerations related to the equipment and the experiment schedule (Sec. 6). The proposal is summarized in Section 7.

2 Physics Motivation

2.1 Overview

In view of the remarks in the Introduction, we consider several interesting questions that motivate us to explore further the measurement of polarization observables in RCS at JLab:

1. Is it indeed true that the RCS reaction proceeds through the interaction of the photons with a single quark?
2. What information can be learned about the structure of the proton from new measurements of the polarization observables and how is this structure related to that measured in other exclusive reaction?
3. At what kinematic scale is factorization into hard and soft process valid?

In order to present a framework for addressing these issues, we next present discussions of three reaction mechanisms: the pQCD, handbag, and Regge exchange mechanisms.

2.2 pQCD Mechanism

The traditional framework for the interpretation of hard exclusive reactions has been perturbative QCD (pQCD) [15]. This is based in part on the observation that the onset of scaling in Deep Inelastic Scattering (DIS) occurs at the relative low scale of $Q^2 \sim 1$–2 $(\mathrm{GeV/c})^2$, thereby giving rise to expectations that pQCD might also be applicable to the exclusive processes in the range of a few $(\mathrm{GeV}/c)^2$. The pQCD approach to RCS [1, 2, 3, 4] is shown in Fig. 2.2, where it is seen that the three valence quarks are active participants in the hard subprocess, which is mediated by the exchange of two hard gluons. The soft physics is contained in the so-called valence quark distribution amplitudes. The pQCD mechanism leads naturally to the so-called constituent counting rules for exclusive processes:

$$\frac{d\sigma}{dt} = \frac{f(\theta_{cm})}{s^n}, \tag{2}$$

where n is related to the number of active constituents in the reaction [16, 17]. Indeed, the observation that many exclusive reactions, such as elastic electron scatter, pion photoproduction, and RCS, approximately obey Eq.2 has led to the belief that the pQCD mechanism dominates at experimentally accessible energies. There seems to be little theoretical disagreement that the pQCD mechanism dominates at sufficiently high energies [18]; however, there is no consensus on how high is "sufficiently high." Indeed, despite the observed scaling, absolute cross sections calculated using the pQCD framework are very often low compared to existing experimental data, sometimes by more than an order of magnitude. Moreover, several recent JLab experiments that measure polarization observables also disagree with the predictions of pQCD. In the G_E^p experiment [19, 20] the slow falloff of the Pauli form factor $F_2(Q^2)$ up to Q^2 of 5.5 $(\mathrm{GeV}/c)^2$ provides direct evidence that hadron helicity is not

conserved, contrary to predictions of pQCD. Similar findings were made in the π^0 photoproduction experiment [21], where both the non-zero transverse and normal components of polarization of the recoil proton are indicative of hadron helicity-flip, which is again contrary to the predictions of pQCD. Finally, in the recently completed RCS experiment, E99-114, the preliminary analysis of the longitudinal polarization transfer K_{LL} (which will be defined precisely below) shows a value which is large and positive, contrary to the pQCD prediction which is negative. Moreover, the E99-114 data are consistent with a scaling factor $n \approx 8$ rather than the value $n = 6$, which is expected from pQCD and was consistent with earlier, less precise data [14] (see Fig. 2.2). For all these reasons, we conclude pQCD is not the correct mechanism for interpreting exclusive reactions at accessible energies and instead seek a description in terms of the handbag mechanism.

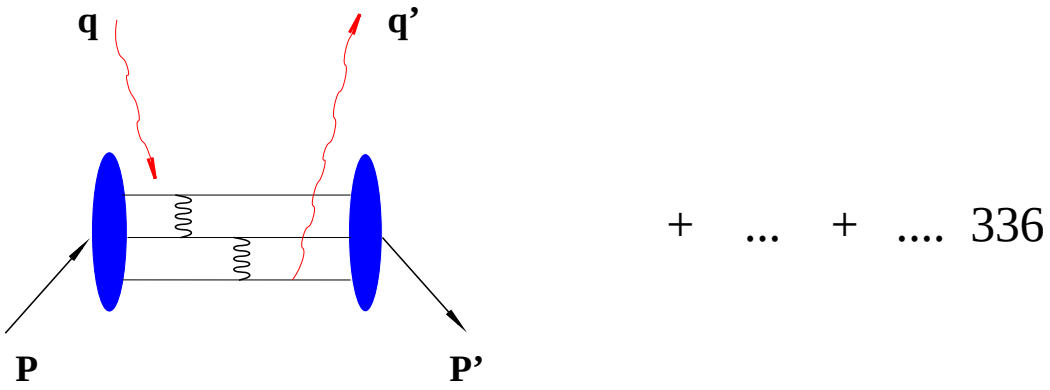

Figure 2: Two gluon exchange pQCD diagram (plus about 336 similar) for RCS.

2.3 Handbag Mechanism

The handbag mechanism offers new possbilities for the interpretation of hard exclusive reactions. For example, it provides the framework for the interpretation of so-called deep exclusive reactions, which are reactions initiated by a high-Q^2 virtual photon. The application of the formalism to RCS (see Fig. 4) was initially worked out to leading order (LO) by Radyushkin [5] and subsequently by Diehl [6]. More recently next-to-leading-order (NLO) contributions have been worked out by Huang and Kroll [7]. The corresponding diagram for elastic electron scattering is similar to Fig. 4, except that there is only one external virtual photon rather than two real photons. In the handbag approach, the hard physics is contained in the scattering from a single active quark and is calculable using pQCD and QED: it is just Compton scattering from a structureless spin-1/2 particle. The soft physics is contained in the wave function describing how the active quark couples to the proton. This coupling is described in terms of GPD's. The GPD's have been the subject of intense experimental and theoretical activity in recent years [23, 24]. They represent "superstructures" of the proton,

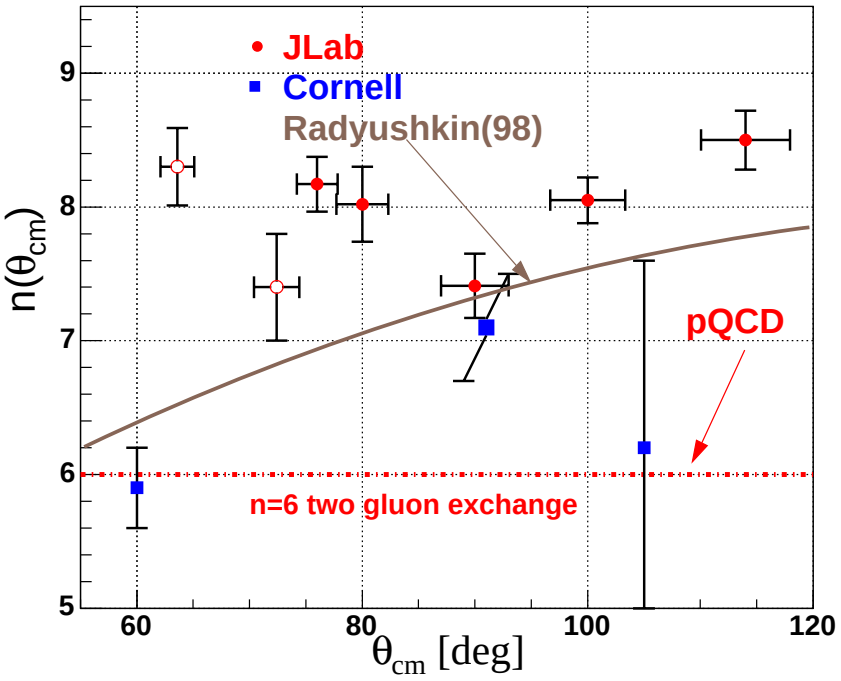

Figure 3: Scaling of the RCS cross sections at fixed θ_{cm}. The open and closed circles are from E99-114. The squares are from the Cornell experiment [14]. The data from E99-114 are consistent with an angle-independent value of $n = 8$, which is inconsistent with the pQCD prediction and the constituent counting rule. The curve is a prediction from Radyushkin based on the handbag model [5]

from which are derived other measurable structure functions, such as parton distribution functions (PDF) and form factors. To NLO, only three of the four GPD's contribute to the RCS process: $H(x, \xi = 0, t)$, $\hat{H}(x, \xi = 0, t)$, and $E(x, \xi = 0, t)$. Since the photons are both real, the so-called skewness parameter ξ=0, reflecting the fact that the momentum absorbed by the struck quark is purely transverse. In the handbag formalism, the RCS observables are new form factors of the proton that are x^{-1}-moments of the GPD's:

$$
\begin{aligned}
R_{_V}(t) &= \sum_a e_a^2 \int_{-1}^{1} \frac{dx}{x} H^a(x, 0, t), \\
R_{_A}(t) &= \sum_a e_a^2 \int_{-1}^{1} \frac{dx}{x}\, sign(x)\, \hat{H}^a(x, 0, t), \\
R_{_T}(t) &= \sum_a e_a^2 \int_{-1}^{1} \frac{dx}{x} E^a(x, 0, t),
\end{aligned}
$$

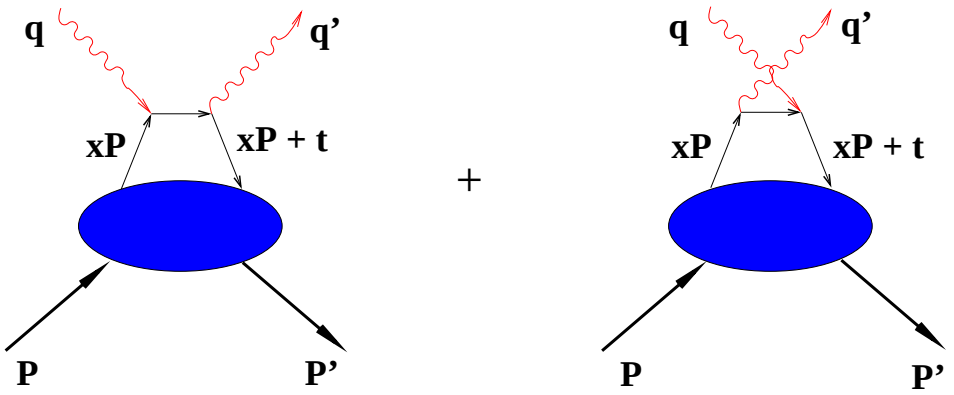

Figure 4: The handbag diagram for RCS.

where e_a is the charge of the active quark and the three form factors are, respectively, the vector, axial vector, and tensor form factors. The corresponding form factors for elastic electron or neutrino scattering are given by the x^0-moments of the same GPD's:

$$\begin{aligned} F_{_1}(t) &= \sum_a e_a \int_{-1}^{1} dx\, H^a(x,0,t), \\ G_{_A}(t) &= \sum_a \int_{-1}^{1} dx\, sign(x)\, \hat{H}^a(x,0,t), \\ F_{_2}(t) &= \sum_a e_a \int_{-1}^{1} dx\, E^a(x,0,t), \end{aligned}$$

where the three quantities are, respectively, the Dirac, axial, and Pauli form factors. On the other hand, the $t = 0$ limit of the GPD's produce the PDF's:

$$\begin{aligned} H^a(x,0,0) &= q^a(x), \\ \hat{H}^a(x,0,0) &= \Delta q^a(x) \\ E^a(x,0,0) &= 2\frac{J^a(x)}{x} - q^a(x), \end{aligned} \tag{3}$$

where J^a is the total angular momentum of quark flavor a and is not directly measurable in DIS.

In the handbag factorization scheme, the RCS helicity amplitudes are related to the form factors by

$$M_{\mu'+,\mu+}(s,t) = 2\pi\alpha_{em}\left[T_{\mu'+,\mu+}(s,t)(R_{_V}(t) + R_{_A}(t)) + T_{\mu'-,\mu-}(s,t)(R_{_V}(t) - R_{_A}(t))\right],$$

$$M_{\mu'-,\mu+}(s,t) \;=\; 2\pi\alpha_{em}\frac{\sqrt{-t}}{m}\left[T_{\mu'+,\mu+}(s,t)+T_{\mu'-,\mu-}(s,t)\right]R_{_T}(t),$$

where μ, μ' denote the helicity of the incoming and outgoing photons, respectively. The signs on M and T refer to the helicities of the proton and active quark, respectively. This structure of the helicity amplitudes leads to a simple interpretation of the RCS form factors: $R_{_V} \pm R_{_A}$ is the response of the proton to the emission and reabsorption of quarks with helicity in the same/opposite direction of the proton helicity, and $R_{_T}$ is directly related to the proton helicity-flip amplitude [7].

These equations leads to expressions relating RCS observables to the form factors. The most important of these experimentally are the spin-averaged cross section and the recoil polarization observables. The spin-averaged cross section factorizes into a simple product of the Klein-Nishina (KN) cross section describing the hard scattering from a single quark and a sum of form factors depending only on t [5, 6]:

$$\frac{d\sigma/dt}{d\sigma_{\rm KN}/dt} \;=\; f_{_V}\left[R_{_V}^2(t) \;+\; \frac{-t}{4m^2}R_{_T}^2(t)\right] + (1-f_{_V})R_{_A}^2(t)\,, \tag{4}$$

For the the interesting region of large $p_\perp$, the kinematic factor $f_{_V}$ is always close to 1. Consequently the unpolarized cross sections are largely insensitive to $R_{_A}$, and the left-hand-side of Eq. 4 is nearly s-independent at fixed t. The recent calculations to NLO, which take into account both photon and proton helicity-flip amplitudes, do not change this prediction in any appreciable way [7]. One of the primary goals of E99-114 was to test this relationship as well as to determine the vector form factor $R_{_V}$, and our results are shown in Fig. 2.3. The longitudinal and transverse polarization transfer observables, $K_{_{LL}}$ and $K_{_{LT}}$, respectively, are defined by

$$K_{_{LL}}\frac{d\sigma}{dt} \;\equiv\; \frac{1}{2}\left[\frac{d\sigma(\uparrow\downarrow)}{dt}-\frac{d\sigma(\uparrow\downarrow)}{dt}\right] \qquad K_{_{LT}}\frac{d\sigma}{dt} \;\equiv\; \frac{1}{2}\left[\frac{d\sigma(\uparrow\rightarrow)}{dt}-\frac{d\sigma(\downarrow\rightarrow)}{dt}\right] \tag{5}$$

where the first arrow refers to the incident photon helicity and the second to the recoil proton helicity ($\uparrow$) or transverse polarization ($\rightarrow$). The induced polarization of the recoil proton normal to the scattering plane, $P_{_N}$, is defined by

$$P_{_N}\frac{d\sigma}{dt} \;\equiv\; \frac{1}{2}\left[\frac{d\sigma(\uparrow)}{dt}-\frac{d\sigma(\downarrow)}{dt}\right] \tag{6}$$

and is independent of the incident photon polarization. Here $\uparrow$ and $\downarrow$ denote the component of polarization up and down, respectively, with respect to the scattering plane. With definitions of two additional parameters

$$\beta \;=\; \frac{2m}{\sqrt{s}}\,\frac{\sqrt{-t}}{\sqrt{s}+\sqrt{-u}} \qquad \kappa(t) \;=\; \frac{\sqrt{-t}}{2m}\,\frac{R_{_T}(t)}{R_{_V}(t)}\,, \tag{7}$$

the three polarization observables are approximately related to the form factors by the expressions [6, 7]

$$K_{LL} \approx K_{LL}^{\rm KN} \frac{R_A(t)}{R_V(t)} \frac{1-\beta\kappa(t)}{1+\kappa^2(t)} \qquad \frac{K_{LT}}{K_{LL}} \approx \kappa(t) \frac{1+\beta\kappa^{-1}(t)}{1-\beta\kappa(t)} \qquad P_N \approx 0\,, \tag{8}$$

where $K_{LL}^{\rm KN}$ is the longitudinal asymmetry for a structureless Dirac particle. These formulas do not include small gluonic corrections, which are discussed in Ref. [7].

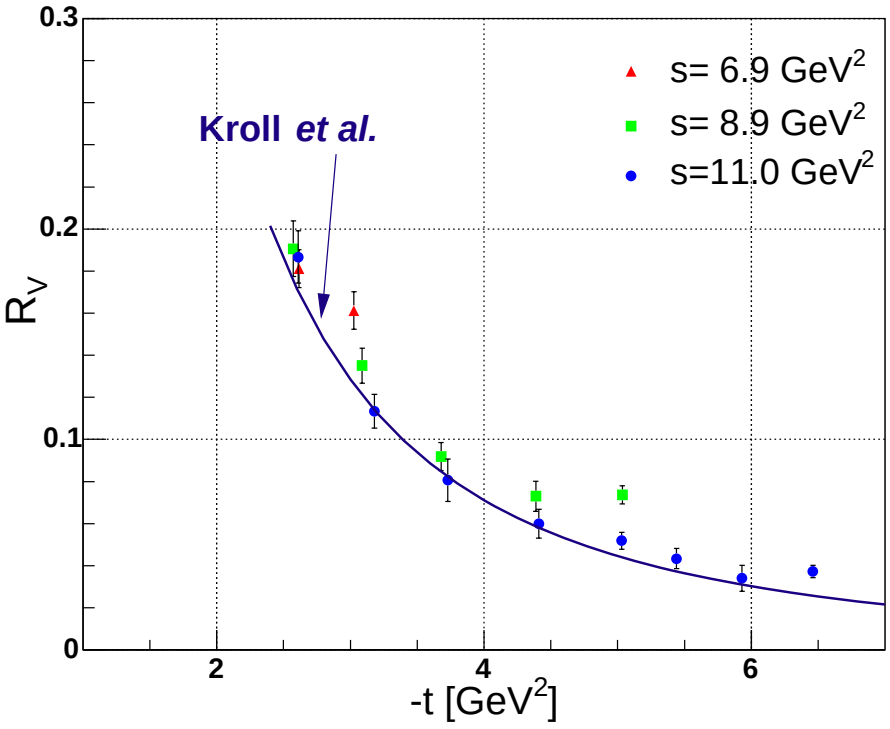

Figure 5: Extracted RCS form factor R_V from E99-114. The solid line is a calculation due to Kroll *et al.*, using GPD's that have been optimized to fit F_1.

These expressions show that measurements of K_{LL} and K_{LT}, when combined with measurements of $d\sigma/dt$ from E99-114, allow determinations of all three form factors. They also show that two very important pieces of information follow directly from the spin asymmetries: K_{LL} and K_{LL}/K_{LT}, which are directly related to the form factor ratios R_A/R_V and R_T/R_V, respectively.

From the relationships connecting RCS form factors to PDF's, Eq. 3, the ratio R_A/R_V is related to $\Delta q^a(x)/q^s(x)$. For RCS, the e_a^2-weighting of the quark flavors means that u quarks will dominate the reaction. Moreover, at moderate-to-high $-t$, the contributions to the form-factor integral are concentrated at moderate-to-high x, where the valence quarks dominate.

Therefore, the K_{LL} asymmetry has direct information on $\Delta u(x)/u(x)$ in the valence region. Obtaining this kind of information is one of the key justifying physics goals for a possible 12 GeV upgrade of JLab.

From the correspondence between RCS and electron scattering form factors, there is expected to be a close relationship between R_T/R_V and F_2/F_1 [7]. The JLab G_E^p experiments [19, 20] have shown that F_2/F_1 falls as $1/\sqrt{-t}$ rather than as $1/t$, the latter being predicted by pQCD. It will be an important check on the theoretical interpretation of F_2/F_1 to see if R_T/R_V behaves in a similar way. In the current context, this means that the parameter $\kappa(t)$, and therefore K_{LT}/K_{LL}, would be nearly independent of t. We propose to investigate this in the proposed experiment, up to $-t = 5$ /(GeV/c)^2. The results from E99-114 at $-t = 4$ are consistent with $R_T/R_V \approx (0.6\pm\ 0.3)F_2/F_1$. Although the uncertainties are large, this result suggests that R_T/R_V may fall more rapidly with $-t$ than F_2/F_1. One of the goals of the proposed experiment is to obtain better precision on K_{LT}.

Finally, we note that the quantity P_N is predicted to vanish to NLO, except for possible gluonic contributions, which involve additional (unknown) soft form factors [7]. These contributions have been estimated to contribute no more than about 0.03 to P_N. An accurate experimental determination of P_N will be helpful in obtaining better estimates of the gluonic contributions to both K_{LL} and K_{LT}.

2.4 Regge Exchange Mechanism

When s, $-t$, and $-u$ are not sufficiently large, then the factorization into hard and soft process may not apply, in which case neither the pQCD nor the handbag approach is valid. An alternative approach has been proposed by Laget [8] based on Vector Meson Dominance (VMD). In the VMD approach, the photon fluctuates into a vector meson, which then interacts with the target via t-channel exchange of mesons (which dominates at low t or forward angles) or u-channel exchange of baryons (which dominates at low u or backward angles). The open question is how high t or u must be in order that the VMD mechanism becomes small compared to the handbag mechanism. The VMD model has had recent successes even at moderately large t. For example the VMD model is able to fit the observed low value of the G_E^p form factor [20] at -t = 5.6 (GeV/c)^2 [25].

Real and Virtual Compton Scattering were studied in a model based on Regge trajectories and two-gluon exchange by F. Cano and J.-M. Laget [8]. The parameters of the model were "tuned" by fitting data from vector meson photonproduction [26, 27], giving rise to predictions for the cross section and spin observables in RCS involving only a single free parameter, the radiative decay constant of the ρ meson. Given the close agreement over much of the kinematic range between the handbag and VMD predictions, they point out that at presently accessible momentum transfer, the contribution to RCS from the hadronic component of the photon is not negligible (see review [28]). For example the predicted longitudinal polarization transfer (see Fig. 1) A_{LL} is positive, close to the prediction of the handbag approach at θ_p^{cm} below 140°, and close to the result from E99-114. However, it

strongly deviates from the handbag prediction at larger angles, where the u-channel exchange of baryons becomes dominant.

2.5 Additional Remarks

It is important to realize that the issues posed at the start of this section are not limited to the RCS reaction. Indeed, they are questions that need to be addressed by all studies of the proton using exclusive reactions in the hard scattering regime. The old paradigm for addressing these questions was the pQCD mechanism and the distribution amplitudes. It is quite likely that the new paradigm will be the handbag mechanism and GPD's. In any case, the reaction mechanism needs to be tested, not only over a wide range of kinematic variables but also over a wide range of different reactions. Of these, RCS offers the best possibility to test the mechanism free of complications from additional hadrons.

It is also important to realize that any evidence for nonzero K_{LT} and P_N is evidence for hadron helicity flip. Such evidence has already been seen in the G_E^p/G_M^p experiment, as discussed above. Independent of whether the handbag formalism is the correct one, it is quite likely that there is a very close relationship between K_{LT}/K_{LL} and F_2/F_1, and it is important to discover what that relationship is.

2.6 Summary of Physics Goals

We propose measurements of the spin asymmetries K_{LL}, K_{LT}, and P_N at an incident photon energy of 4.3 GeV (s=8.95 (GeV/c)^2 at three different scattering angles corresponding to $-t$ in the range 2.39 to 4.88 (GeV/c)^2. The specific physics goals are as follows:

1. Provide a stringent test of the notion that the RCS reaction proceeds via the interaction of the photons with a single quark.
2. Determine the form factor ratio R_T/R_V from measurments of K_{LT}/K_{LL} and correlate these measurements with the corresponding values of F_2/F_1 determined from elastic electron scattering.
3. Determine the form factor ratio R_A/R_V.
4. Measure P_N in order to aid in the further development of the theoretical framework.

The overall statistical precision with which we will address these physics goals will be discussed in Sec. 5.

3 Experimental Setup

The proposed experiment will study the scattering of polarized photons from a liquid hydrogen target, illustrated in Fig. 6. The scattered photon will be detected in the BigCal calorimeter installed at a distance to match the acceptance of the HRS-left (HMS), which will be used to detect the recoiling proton.

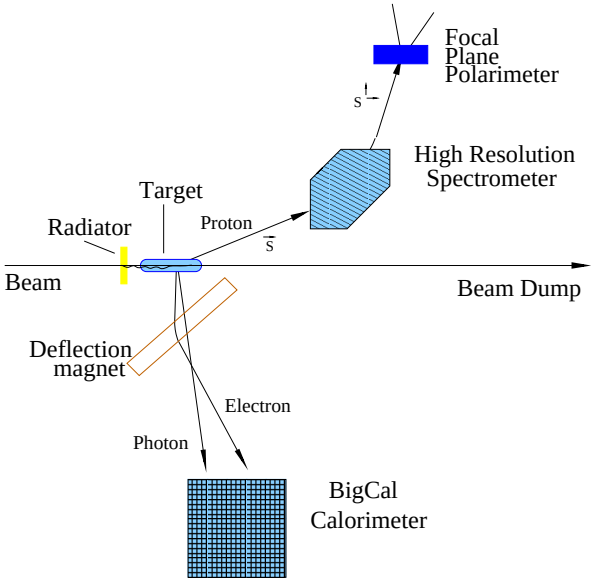

Figure 6: The experimental setup.

3.1 The CEBAF Polarized Beam

Based on our experience with E99-114, we assume an incident electron beam of intensity up to 100 μA in Hall A (60 μA in Hall C) and with 80% polarization. Such currents and polarizations have already been delivered over long periods of time using the strained GaAs source at Jefferson Lab. The beam polarization will be measured to a systematic uncertainty of 3% with the Möller polarimeter. The large cross section and helicity asymmetry for π° photoproduction, as determined from E99-114, will allow a check a product of the electron beam polarization and FPP analysing power continuously during data taking at fixed kinematic conditions with large θ_p^{cm}. Continuous monitoring of the beam polarization also can be done by using the Compton polarimeter.

3.2 The Liquid Hydrogen Target and the Radiator

The experiment will utilize the standard Hall A/C liquid hydrogen (LH2) target with a 15-cm long machined cell, which was successfully employed for many experiments in JLab.

The radiator will be mounted on the cell block about 4 inches upstream of the cell entrance window. The short distance between the target and radiator helps to avoid background produced from Al walls of the target.

3.3 The Deflection Magnet

It was shown in E99-114 experiment that the deflection magnet provides sufficient separation of electron and photon elastic scattering events (see Fig. 7). The magnet obviates the need for a veto detector, which in turn allows us to utilize at least ten time higher photon intensity. The deflection magnet for the proposed experiment will be the same one constructed for and used in E99-114 (see Fig. 8).

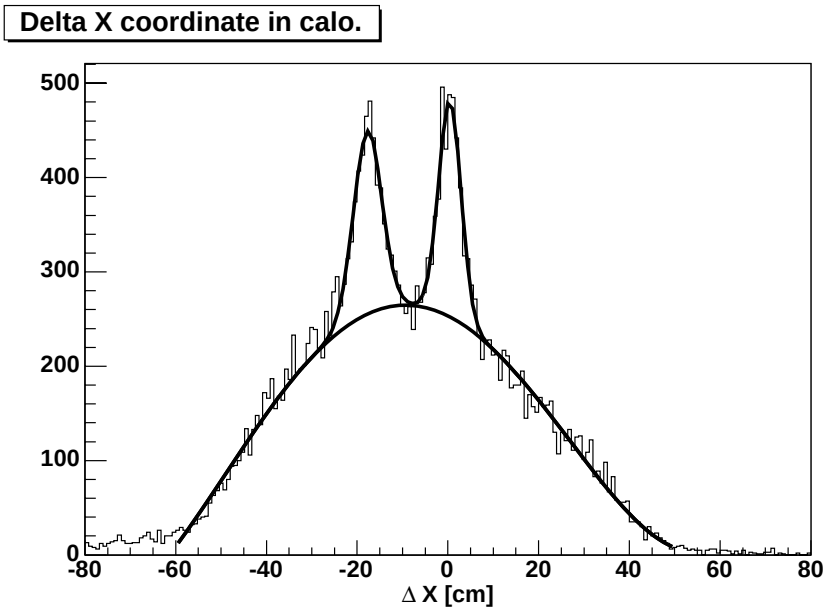

Figure 7: Experimental data from E99-114 at the kinematics $E = 4.3\,GeV$ and θ_{γ}^{lab}= 57^{o} showing the event distribution in the horizontal plane. The peak at coordinate ΔX = 0 corresponds to the RCS events. The peak at ΔX = -18 cm corresponds to the elastic electron scattering, which is offset from the RCS peak due to the deflection magnet.

3.4 The Photon Calorimeter

The photon calorimeter is the main piece of instrumentation to be constructed and installed. We are participating in the construction of the BigCal calorimeter for the GEP-III experiment in Hall C [29]. This calorimeter consists of 1750 lead glass blocks of type TF-1. There are 32 columns and 56 rows of blocks. Figure 20 shows the front and top view of the

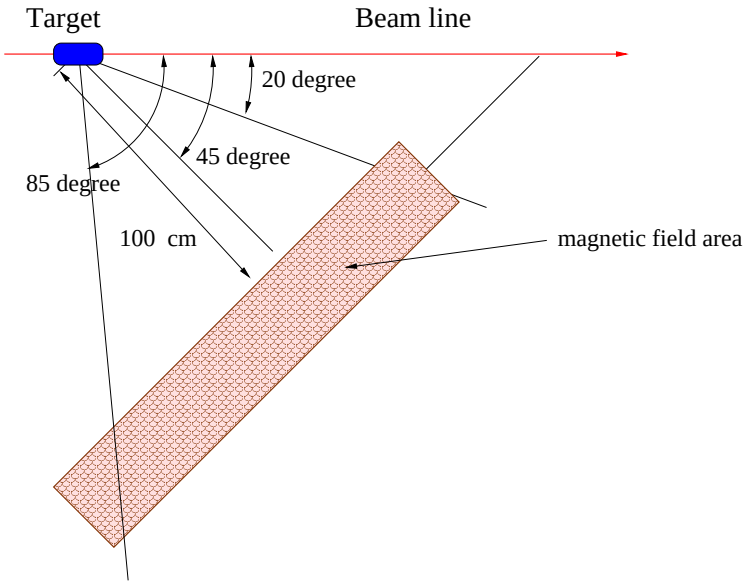

Figure 8: Layout of the deflection magnet.

calorimeter and support structure and the front end electronics. It can be moved into the hall without disconnecting the calorimeter from the front end electronics.

The position of the photon arm will be adjusted for each kinematics to match the HRS. As was successfully realized in E99-114, the movement of the calorimeter will be achieved by using the overhead crane and manual pulling of the cable train. Less than two hours (beam off to beam on) was used in a typical access into the hall for movement of the calorimeter.

3.5 The Data Analysis Procedure

We describe below the simplified version of the analysis procedure. The correlation between expected and observed positions of the photon on the front face of calorimeter is the primary parameter used in analysis of the RCS experiment. The expected photon position is calculated from the measured value of the proton momentum, its direction and position at the target. An example of such kinematical correlation from E99-114 is shown in Fig. 9. Three types of events are presented: RCS events, which are concentrated at the center ΔX = ΔY = 0; the photopion events, which have wider distribution in both directions ΔX and ΔY; and the electron scattering events, which are peaked at ΔX = - 22 cm, ΔY = 0. The events in the region of $\pm 2\sigma$ around the Compton peak are called the correlated events. and the number of events is N_{corr}. The pion event sample can be made with events located above $\Delta Y = 2\sigma_y$ and below the $\Delta Y = -2\sigma_y$ or with events which have $\Delta X > 2\sigma_x$. Figure 10 shows the ΔY-distribution for events with $-2\sigma_x < \Delta X < 2\sigma_x$ when the shape of pion sample is taken from $\Delta X > 2\sigma_x$.

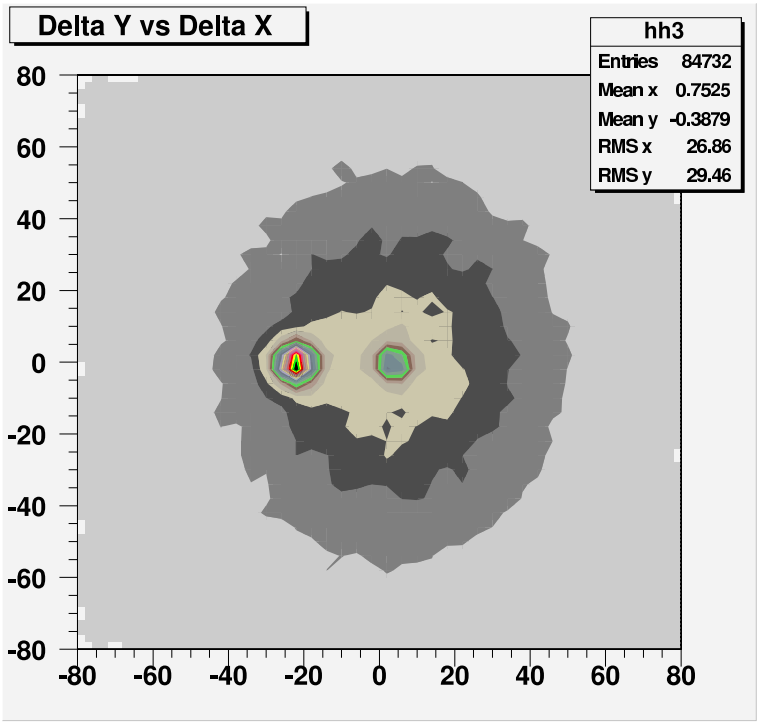

Figure 9: Experimental data from E99-114 at the kinematics $E = 3.23\,GeV$ and θ_p^{cm}=98^o showing the event distribution in the $\Delta X - \Delta Y$ plane.

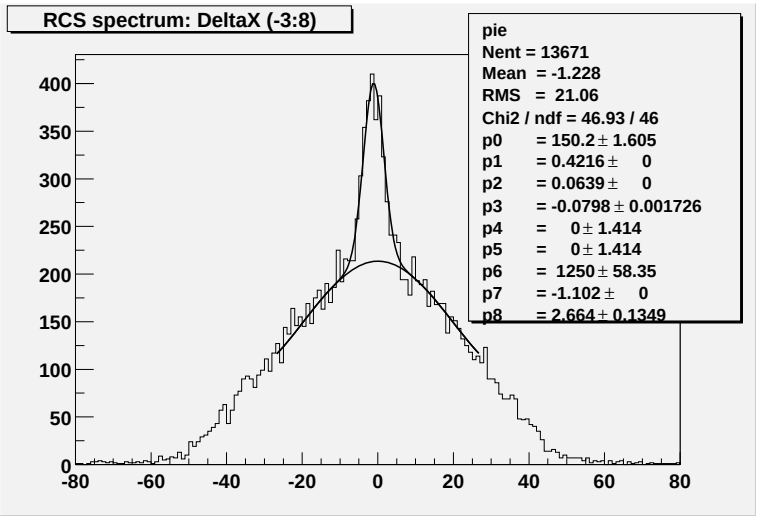

Figure 10: Experimental data from E99-114 at the kinematics $E = 3.23\,GeV$ and θ_p^{cm}=98^o showing the event distribution in ΔY for the cut $-3 < \Delta X < 8$.

3.6 The Focal Plane Polarimeter

The polarization of the recoil proton is measured in the focal plane polarimeter (FPP). Figure 11 shows layout of the FPP with two analyzers, as used in E99-114. Figure 12

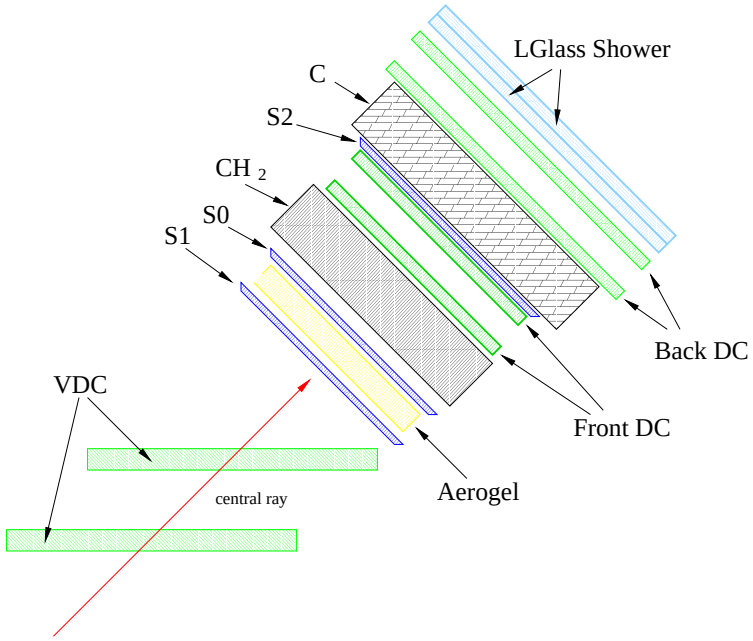

Figure 11: The structure of the detector package in the HRS with the focal plane polarimeter. The vertical drift chamber (VDC), the front drift chambers and back drift chambers are used in FPP tracking analysis. The aerogel Cherenkov counter is used for pion rejection.

shows the notation of the components of the proton polarization at the target. They are P_l (longitudinal), P_t (tranvserse, in the reaction plane), and P_n (normal to the reaction plane). The first two are dependent on the beam helicity, whereas the last is independent. The polarization at the FPP can be found in first approximation (assuming that the HRS is a simple dipole) from expressions

$$P_t^{fpp} = P_t, \qquad P_l^{fpp} = P_l \cdot \cos\chi - P_n \cdot \sin\chi$$
$$\text{and} \qquad P_n^{fpp} = P_l \cdot \sin\chi + P_n \cdot \cos\chi$$

where χ is the spin precession angle relative to the direction of the momentum given by $\chi = 86^\circ \cdot E_p\ (\text{GeV})\ [\theta_{bend}/45^\circ]$. For example, for a proton with momentum 3.0 GeV/c the average precession angle in the HRS is 270°, so the longitudinal component of the proton polarization alone defines the value of the P_n^{fpp}. The P_n^{fpp} has a helicity dependent part $P_{n,h}^{fpp}$ related to P_l and a helicity independent one related to P_n.

Figure 13 demonstrates the principles of operation of the FPP. The method is based on the scattering of the proton from the analyzer material. The number of protons which scatter

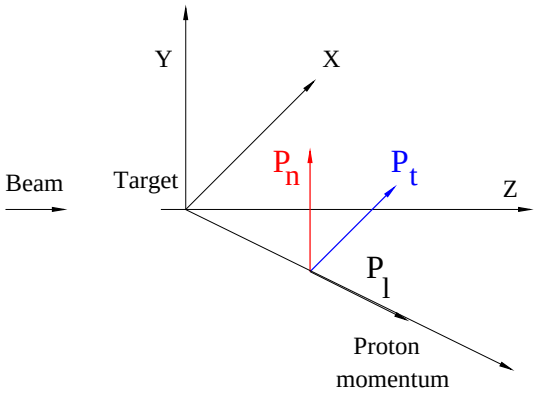

Figure 12: The definition of the polarization components at the target.

from the analyzer can be expressed as a function of their polar and azimuthal angles, θ and ϕ, respectively, as

$$N(\phi,\theta) \;=\; N_p(\theta)\left[1 \;+\; h\cdot A_y(\theta)\cdot(P_t^{fpp}\cdot\sin\phi \;-\; P_{n,h}^{fpp}\cdot\cos\phi) \;+\; A_y(\theta)\cdot(P_n^{fpp} - P_{n,h}^{fpp})\cos\phi\right]$$

where $h = \pm$ is the sign of the beam helicity; $A_y(\theta)$ is the analyzing power, which is an empirical function of θ, the proton momentum, and structure of the analyzer material; and the N_p^h is the total number of protons incident on the polarimeter. The FPP allows a determination of the two components of the polarization perpendicular to the proton momentum in the focal plane - P_t^{fpp} and P_n^{fpp}. Since the normal component of the proton polarization P_n is helicity-independent, all three polarization components at the target can be determined as

$$P_n \;=\; (P_n^{fpp} - P_{n,h}^{fpp})/\cos\chi, \quad P_l \;=\; P_{n,h}^{fpp}/\sin\chi, \quad P_t \;=\; P_t^{fpp}$$

3.6.1 Figure-of-Merit of the Focal Plane Polarimeter

The statistical accuracy of the polarization measurement δP is expressed as

$$\delta P \;=\; \sqrt{2/\left[\epsilon A_y^2\cdot(N_p^+ + N_p^-)\right]},$$

where ϵ (the FPP efficiency) is the fraction of incident protons with scattering angle θ in the range of large analyzing power; A_y is the average analyzing power over the same range of scattering angles; and $N_p^{\pm}$ is the number of incident protons for each photon helicity. The Figure-of-Merit (FOM), ϵA_y^2, as well as total events $(N_p^+ + N_p^-)$, determine the statistical accuracy of the asymmetry measurement. The analyzing power depends on the proton momentum and polarimeter structure (see for example reference [30]). It is a function of the transverse component of the proton momentum after the scattering $p_{trans} \;=\; p_p\sin\theta$. The

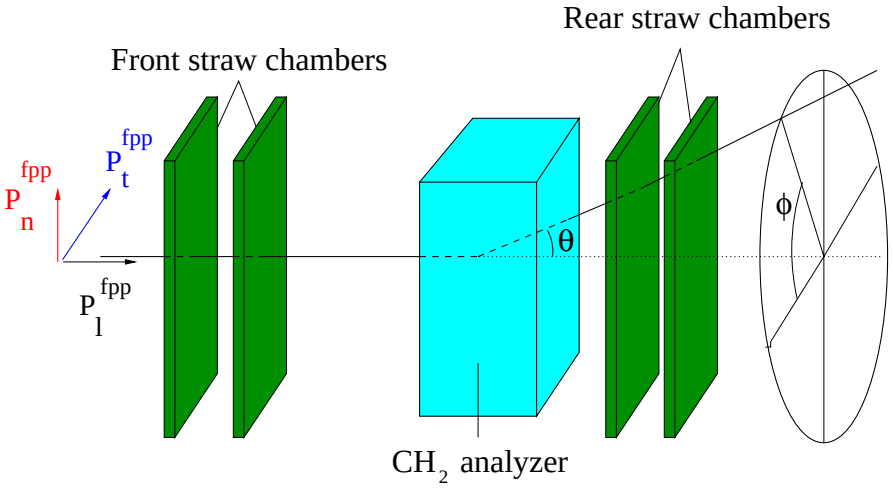

Figure 13: The operation of the Focal Plane Polarimeter.

two most common materials used as an analyzer are Carbon and Polyethylene (CH_2). The FOM for CH_2 is 1.25 larger than that of Carbon [31]. Moreover the maximum A_y is always located at $p_{trans} \sim 0.30$ GeV/c. For optimized thickness of the analyzer, the value of the maximum was described by $A_y = 0.40/p_p$ (GeV/c) for CH_2 analyzer [31].

According to the preliminary analysis of the double-analyzer FPP configuration used in E99-114, the FOM consists of 0.0013 for the CH_2 (thickness = 44 cm) plus an additional 0.0006 for the Carbon analyzer (thickness = 60 cm) at $p_p = 3.0$ GeV/c. These considerations lead to the total FOM of $0.020/p_p^2$ (GeV/c)^2 for two CH_2 analyzers, which we use here for estimates of the required statistics and beamtime.

3.6.2 Calibration of the Proton Polarization

Because the analyzing power is quite sensitive to the polarimeter structure, the practical way to determine the analyzing power is a calibration of the FPP using the recoil protons from elastic scattering of the polarized electrons. Calibrations allow a measure of both the analyzing power and the instrumental asymmetry. In elastic electron scattering the polarization of the recoil proton at the target can be calculated from the following expressions [32, 33]:

$$P_{t,ep} = -\frac{2\sqrt{\tau(1+\tau)}\tan\frac{\theta}{2}}{g^2+\tau\epsilon^{-1}} \cdot g \qquad \text{and} \qquad P_{l,ep} = \frac{2\sqrt{\tau(1+\tau)}\tan\frac{\theta}{2}}{g^2+\tau\epsilon^{-1}} \cdot \frac{(E_i+E_f)\tan\frac{\theta}{2}}{2M_p}$$

where M_p is the proton mass, $E_{i(f)}$ is the initial (final) electron energy, $g = G_E^p/G_M^p$ is the ratio of the proton form factors, $\tau = Q^2/4M_p^2$ with $-Q^2 = 4E_iE_f\sin^2\frac{\theta}{2}$, and $\epsilon^{-1} = 1 + 2(1+\tau)\tan^2\frac{\theta}{2}$. The values of $P_{t,ep}$ and $P_{l,ep}$ determine the $P_{t,ep}^{fpp}$ and $P_{n,ep}^{fpp}$ used

for the calibration process. The beamtime required for FPP calibration with 5% accuracy was between 2 and 10% of that RCS data-taking time.

3.6.3 Analysis of the Helicity Asymmetry in E99-114

E99-114 collected data with polarized photons for the average photon energy of 3.23 GeV and θ_p^{cm} =122°. Figure 14 shows the helicity asymmetry A_h observed in the distribution of recoil protons vs. azimuthal angle in the FPP for elastic electron scattering from the proton. A_h was calculated as

$$A_h(\phi) = \frac{1}{2}\left[\frac{N^+(\phi)}{N_p^+} - \frac{N^-(\phi)}{N_p^-}\right],$$

where $N^{\pm}(\phi)$ is an integral of $N^{\pm}(\phi,\theta)$ over the range $\theta = 3°-20°$. The observed asymmetries for both analyzers are about 0.053. These results were used for calibration of the FPP.

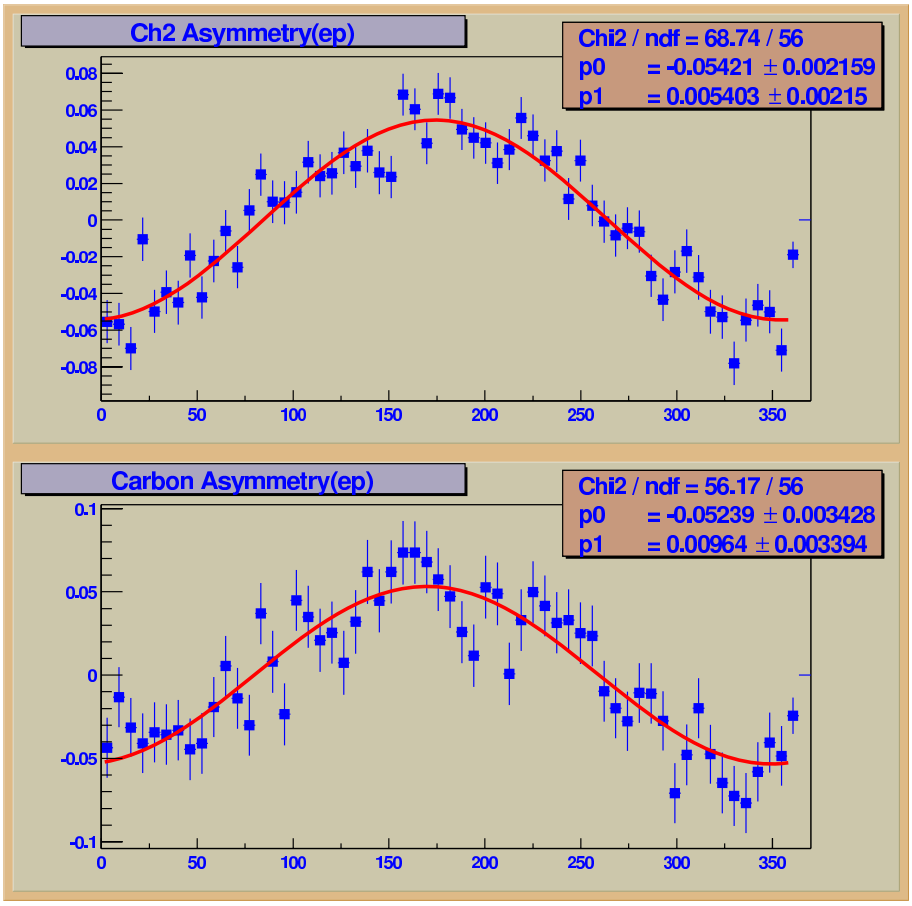

Figure 14: Beam helicity asymmetry for elastic electron scattering from proton.

Figure 15 shows the helicity asymmetry for the π° photoproduction. Figure 16 shows the asymmetry for the kinematically correlated events, where RCS and π° events are mixed in ratio of 1:2. The asymmetries obtained from the above analysis are A_{ep}, A_{π°, and A_{corr} (we

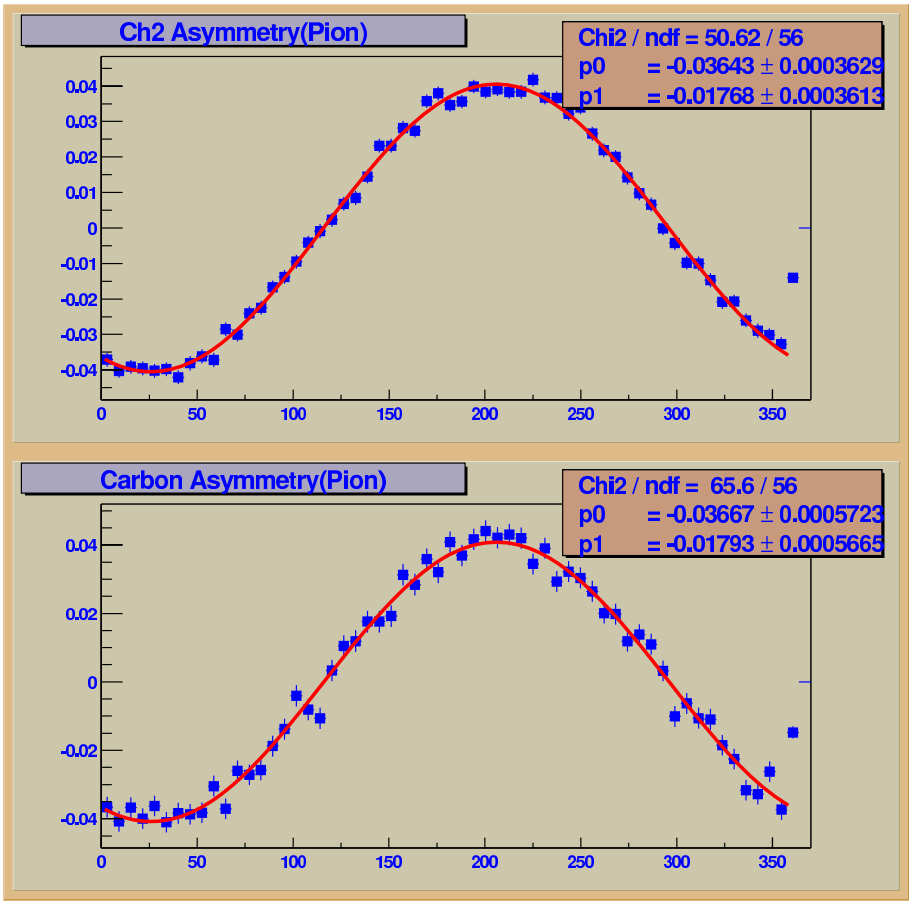

Figure 15: Beam helicity asymmetry for the π° photoproduction from proton.

droped helicity index h in expressions here and below). Each of them has two components, A_t and A_n, denoted on the plots as $P0$ and $P1$, respectively.

The asymmetry for RCS events is determined from the following:

$$A_{_{RCS}} = A_{corr} \cdot D - A_{\pi^\circ} \cdot (D-1)$$

where D is a dilution factor defined as $(N_{\gamma,\pi^\circ} + N_{\gamma,\gamma})/N_{\gamma,\gamma}$ for the kinematically correlated photon-proton events. Because of the large number of π° events, A_{π° is very well determined so that the accuracy of $A_{_{RCS}}$ is determined by the statistical precision of A_{corr}:

$$\delta A_{_{RCS}} = D \cdot \sqrt{2/N_{corr}}$$

The P_t and P_n components of the proton polarization at the FPP for RCS are expressed as

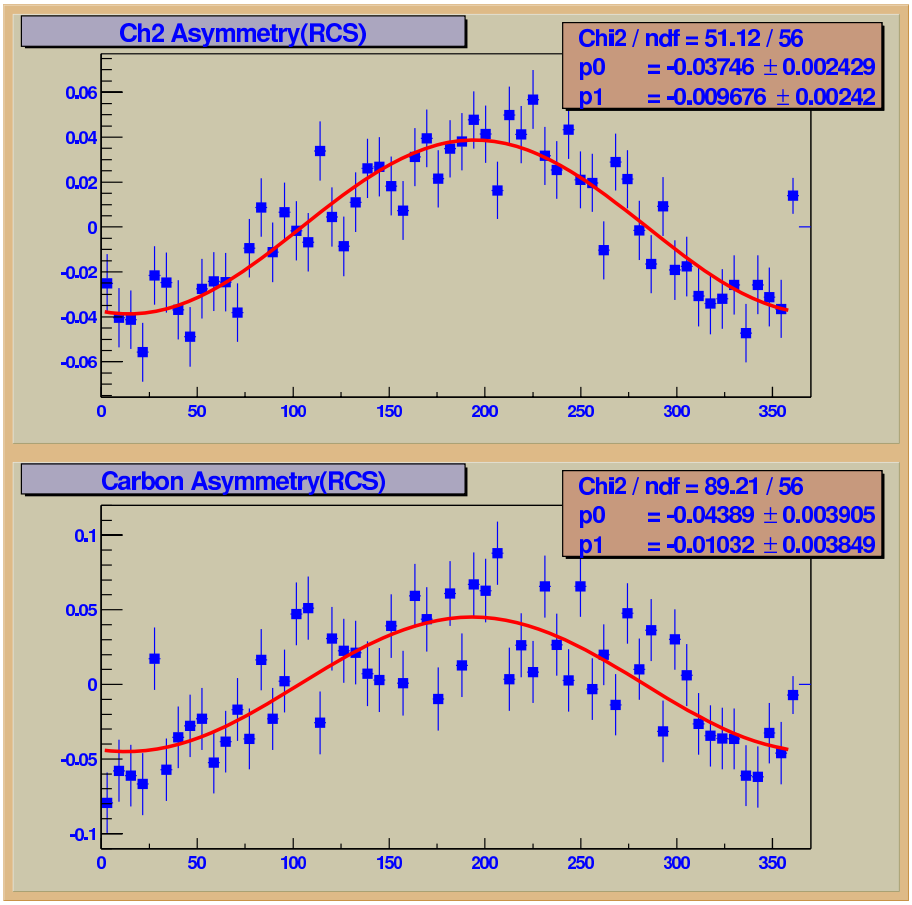

Figure 16: Beam helicity asymmetry for kinematically correlated photon-proton events.

$$P^{fpp}_{t,RCS} = P^{fpp}_{t,ep} \cdot [P0_{corr} \cdot D - P0_{\pi^\circ} \cdot (D-1)] / P0_{ep}$$

$$P^{fpp}_{n,RCS} = P^{fpp}_{t,ep} \cdot [P1_{corr} \cdot D - P1_{\pi^\circ} \cdot (D-1)] / P0_{ep}\,.$$

In the last formula we used the $P0$ component of the asymmetry and $P^{fpp}_{t,ep}$ because it is better determined than $P1$ for the kinematics of our experiment. These formulas determine the magnitude and direction of the proton spin at the FPP in the proton rest frame relative to the direction of the proton momentum in the lab frame.

The preliminary results of E99-114 (averaged from both analyzers and normalized to 100% photon polarization) are

$$P_{l,RCS} = 0.75 \pm 0.11 \quad P_{t,RCS} = -0.10 \pm 0.10$$

3.6.4 Transformation to the CM Frame

The FPP is calibrated based on the polarization of the proton from elastic electron scattering, whose components were calculated relative to the direction of the proton momentum in the lab frame. Therefore the results for RCS are found also relative to the direction of the the proton momentum in the lab frame. The calculations of RCS polarization observables done in the photon-proton cm frame, so the observed experimental proton polarization need to be transfered also to photon-proton cm frame.

The transformation from lab to cm frame can be represented as a rotation of the polarization vector by angle α. The magnitude of the proton polarization is unchanged in the transformation, but the values of the l and t components are changed as follows:

$$\begin{aligned} P^{cm}_{l,RCS} &= P^{lab}_{l,RCS} \cdot \cos\alpha \; - \; P^{lab}_{t,RCS} \cdot \sin\alpha \\ P^{cm}_{t,RCS} &= P^{lab}_{l,RCS} \cdot \sin\alpha \; + \; P^{lab}_{t,RCS} \cdot \cos\alpha \end{aligned}$$

For the kinematics of E99-114 polarization measurements, $\alpha = 20^\circ$ which leads to polarization transfer parameters $K_{LL} = 0.74 \pm 0.11, \quad K_{LT} = 0.16 \pm 0.11$.

4 Proposed Measurements

A longitudinally polarized electron beam of energy 4.8 GeV with current of 60 μA in P1 kinematics and 100 μA in kinematics P2-P3 will be used. The Cu radiator with thickness of 1.3 mm (10% radiation length) will be installed 4 inches upstream of the 15 cm-long liquid hydrogen target. Photons of average energy 89% of the electron beam energy will be used. For such bremsstrahlung photons, the circular polarization is almost equal polarization of the electrons. The recoil proton will be detected in magnetic spectrometer HMS in Hall C for measurement P1. The recoil proton will be detected in magnetic spectrometer HRS-left in Hall A for measurements P2 and P3. The scattered photon will be detected in the large calorimeter BigCal. The components of the polarization of the recoil proton will be measured in the focal plane polarimeters (FPP).

All features of the experimental technique were used in E99-114. The larger size of the BigCal calorimeter will allow the experiment to be done with a larger distance between the target and the calorimeter and consequently a larger luminosity by a factor of 2.5 be used with the same radiation load per lead-glass module. Analysis of the trigger rate and signal amplitude fluctuation due to high rate effect in E99-114 data show that load per block could be **doubled** with no loss of performance for RCS events. The lower beam current in the kinematics P1 was chosen due to a larger solid angle and momentum acceptance of HMS.

4.1 The Kinematics

The central momentum of the proton spectrometer will correspond to the elastic scattering of the photon (or electron) with initial energy 4.3 GeV (about 11% below the beam energy). The overlap of the acceptances of the photon and proton arms will be done the same way as in E99-114: The photon arm has the defining angular acceptance. Figure 17 shows the simulation of the incident photon spectra folded with the combined acceptances of the two arms. The effective photon energy range, which we are going to use in analysis, defined also by the acceptance overlap, is approximately 0.4 GeV or 10% of incident photon energy. The proposed measurements are presented in Table 1, where α is the spin rotation angle for transformation from the laboratory to cm frame.

kin. P#	t, $(\mathrm{GeV}/c)^2$	u, $(\mathrm{GeV}/c)^2$	θ_γ^{lab}, degree	θ_p^{cm}, degree	θ_p^{lab}, degree	E_γ^{lab}, GeV	p_p GeV/c	precession χ, degree	sinχ	α, degree
P1	-2.39	4.00	24.8	70	39	3.00	2.00	127	0.80	39.4
P2	-3.64	3.55	34.9	90	30	2.36	2.72	247	-0.92	29.7
P3	-4.88	2.31	48.3	110	22	1.70	3.41	304	-0.83	21.9

Table 1: The kinematics parameters of the proposed measurements at $s = 8.95$ $(\mathrm{GeV}/c)^2$. P1 is for HMS, P2 and P3 are for HRS.

4.2 Expected Rates

In E99-114 unpolarized data were collected for the average photon energy of 4.3 GeV and θ_p^{cm} in range $70^\circ - 110^\circ$. Table 3 presents the cross section of RCS process at photon energy of 4.3 GeV. The event rates are the products of the luminosity, the cross section, and the acceptances of the detectors, as well all other factors such as DAQ dead time, efficiency of the trigger and the detectors, efficiency of the reconstruction analysis. The rate, N_{RCS} was calculated as:

$$N_{RCS} = \frac{d\sigma}{dt}_{RCS} \frac{(E_\gamma^f)^2}{\pi} \Delta\Omega_\gamma f_{\gamma p} (\frac{\Delta E_\gamma^f}{E_\gamma^f} \frac{t_{rad}}{X_o}) \mathcal{L}_{ep}$$

where $\frac{d\sigma}{dt}_{RCS}$ is the RCS cross section (see Table 2); the factor $\frac{(E_\gamma^f)^2}{\pi}\Delta\Omega_\gamma$ is the range of Δt for the given kinematics, expressed through the energy of the scattered photon and the solid angle of the photon detector; $f_{\gamma p} = 0.4 - 0.7$ is the fraction of events detected for given range of photon energy E_γ^f; $(\frac{\Delta E_\gamma^f}{E_\gamma^f}\frac{t_{rad}}{X_o}) = 0.4/4.3 \cdot 0.13$ is the number of photons per incident electron, including the photons produced in the target and virtual photons; $\mathcal{L}_{ep} = 3.6 \cdot 10^{38}$ $\mathrm{cm}^{-2}\mathrm{sec}^{-1}$ is the electron-proton luminosity for 100 μA beam. The simulated photon spectra for the proposed kinematics is shown in Figure 17.

The Table 2 also shows the dilution factor D defined as $(N_{\gamma,\pi^\circ} + N_{\gamma,\gamma})/N_{\gamma,\gamma}$ for the kinematically correlated photon-proton events and the $f_{\gamma p}$, the phase space factor for the proton arm. The observed calorimeter rate was used to choose experiment luminosity. The

kin. 4#	θ_γ^{lab} degree	-t, $(\mathrm{GeV}/c)^2$	θ_p^{cm}, degree	D	$F_{trigger}$ kHz/msr/μA	$d\sigma/dt$ pb/$(\mathrm{GeV}/c)^2$
4A	22	2.03	63.8	2.13	0.80	456
4B	26	2.57	72.8	1.54	0.53	146
4C	30	3.09	81.1	1.67	0.56	78
4D	35	3.68	90.4	2.75	0.40	40
4E	42	4.39	101.5	2.80	0.51	30
4F	50	5.04	112.1	2.42	0.62	36
4G	57	5.48	119.9	2.83	0.42	54
4H	66	5.93	128.4	3.89	0.30	65

Table 2: The cross section of RCS for 4.3 GeV photon energy. Here D is dilution factor. $F_{trigger}$ is the calorimeter trigger rate at the threshold of 55% of the RCS photon signal.

observed cross section was used for an estimate of the rates in the proposed experiment. We extrapolate the cross section linearly between data points inside the angular region of E99-114. Table 3 presents main parameters of kinematics and the expected RCS events rates for the proposed measurements. The distance between the target and the calorimeter was optimized to match the acceptance of the proton spectrometer, except for the limitation imposed by the space in Hall C in case of P1 kinematics. The resulting solid angle of the photon arm $\Delta\Omega_\gamma^{lab}$ and acceptance factor $f_{\gamma p}$ are shown in the same table.

kin. P#	θ_γ^{lab}, degree	$\Delta\Omega_\gamma^{lab}$, msr	t, $(\mathrm{GeV}/c)^2$	θ_p^{cm}, degree	Dist, m	$f_{\gamma p}$	ν_{RCS} Hz
P1	24.8	4.3	2.39	70	15	0.72	10.
P2	34.9	9.8	3.64	90	15	0.62	2.5
P3	48.3	21.8	4.88	110	10	0.71	2.7

Table 3: The expected rates of RCS events in the proposed experiment.

4.3 Required Statistics

As was shown in Sec. 3, the Figure-of-Merit of the FPP is approximately $\sim 0.020/p_p^2$ $(\mathrm{GeV}/c)^{-2}$. The statistics required for obtaining accuracy of $\Delta P_{n,h}^{fpp}$ with 80% photon beam polarization (which is included in determination of the FOM) can be calculated:

$$N_{_{RCS},required} = 100 \cdot p_p^2 \cdot D/sin^2\chi/(\Delta P_{n,h}^{fpp})^2 \,.$$

Table 4 presents required statistics for each kinematics.

kinematic	P1	P2	P3
$N_{_{RCS}}$, events	0.42M	0.98M	1.7M
$\Delta K_{_{LL}}$	0.07	0.05	0.06
$\Delta P_{_N}$	0.08	0.13	0.09
$\Delta K_{_{LT}}$	0.05	0.05	0.05

Table 4: The statistics and expected statistical accuracy in the proposed experiment. The values of the uncertainties were not adjusted for spin rotation in the transformation between the laboratory and cm systems.

4.4 Optimization of experimental setup

We have chosen to divide the experiment between Halls A and C for the following reason. If the experiment were to run entirely in Hall A, it would require an additional 15 days of beam time, due to 1.5 times larger spin precession in Hall A HRS, as opposed to Hall C HMS. It mades the measurement of $K_{_{LL}}$ time consuming in Hall A for the first kinematic point. Running just one point in Hall C would still not make sense, due to the installation and de-installation times required for the BIGCAL calorimeter, except that two experiments are already expected to run with BIGCAL in Hall C, likely in 2007. These are the Gep-III (E04-108) and the Gep-2gamma (E04-019) experiments. Thus, the first kinematic point can be run along with these experiments, for only the addition of a few days of beam time. It does not make sense to run the entire experiment in Hall C, as the second and the third points would require production time 5 and 12 times longer in Hall C than in Hall A.

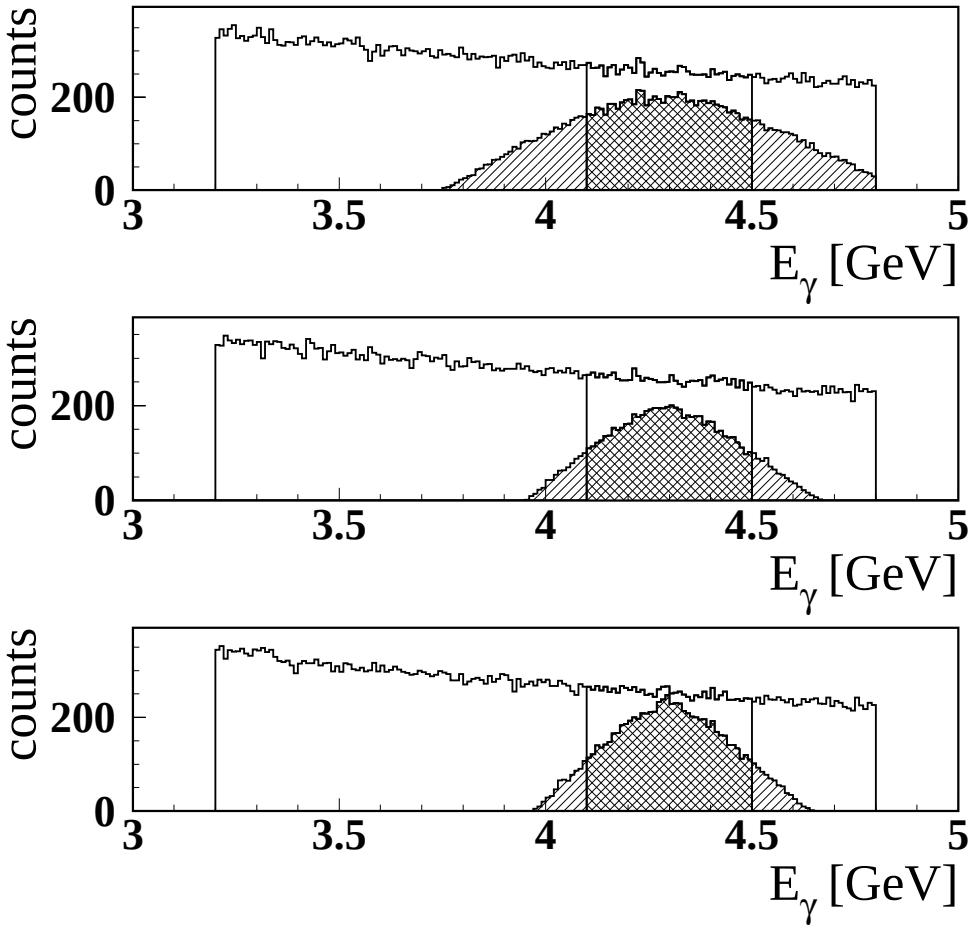

Figure 17: The simulated photon spectra for the proposed kinematics. The photon spectra in coincidence with the proton are shown by dashed area.

5 Expected Results and Beam Time Request

5.1 Expected Results

The purpose of this experiment is to measure the polarization transfer parameters K_{LL}, K_{LT}, and P_N with accuracy sufficient to obtain conclusive evidence on the dominance of the specific reaction mechanism. Another purpose is to determine the form factor ratios: R_A/R_V, which is related to K_{LL}; and R_T/R_V , which is related to K_{LT}/K_{LL}. We propose to obtain the statistical accuracies shown in Table 4, which will lead to the expected results for K_{LL} that are shown in Fig. 18. Similar statistical accuracy is expected for K_{LT} and P_N. Using the handbag formalism to interpret the results of the K_{LL} and K_{LT} measurement, we will extract values for R_A/R_V and R_T/R_V with the expected accuracy shown in Fig. 19.

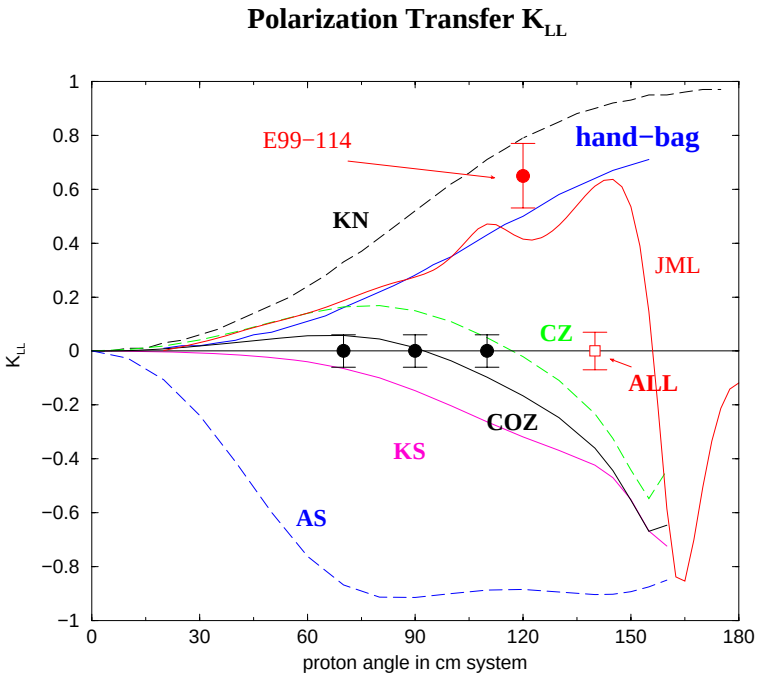

Figure 18: Polarization transfer observable K_{LL} in the RCS process with expected accuracy of the proposed measurements shown as black circles. The open square shows expected accuracy of the experiment [35], which will measure A_{LL} observable at s=9 $(\mathrm{GeV}/c)^2$. The labels on the curves are KN for the asymmetry in the hard sub process; the pQCD calculations [4] with AS for asymptotic distribution amplitudes, with CZ for Chernyak-Zhitnitsky [36], with COZ for Chernyak-Ogloblin-Zhitnitsky [37], with KS for King-Sachrajda [38]; hand-bag for calculations in Soft overlap approach [7], JML for calculation in Regge approach [8] .

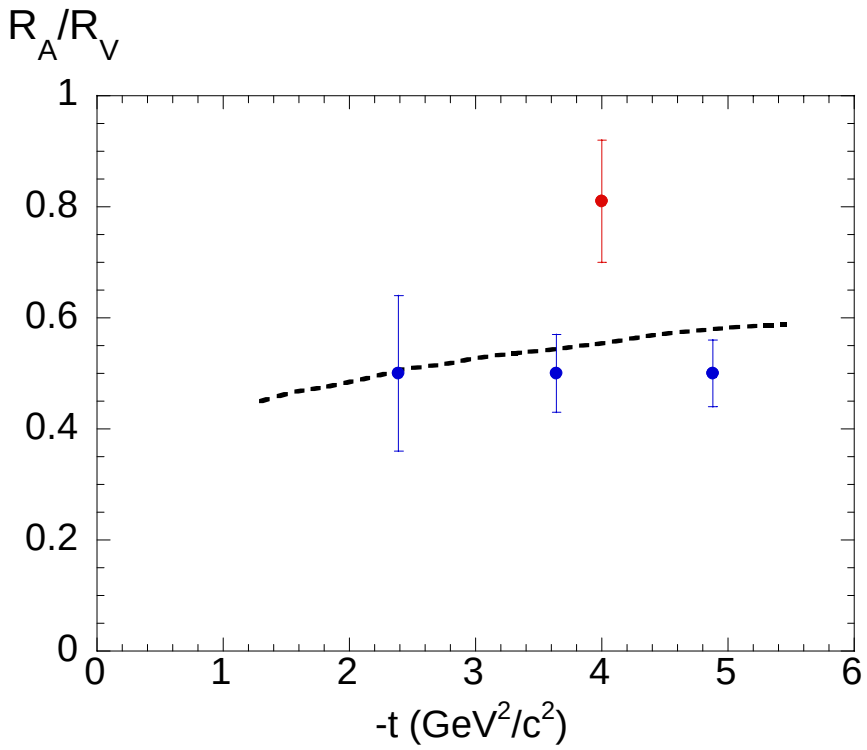

Figure 19: Expected results for the form factor ratios R_A/R_V. The point at $-t$=4 (GeV/c)^2 is the expected result from E99-114. The curve is prediction of Ref. [7].

5.2 Beam Time Request

The proposed experiment will be done at one beam energy of 4.8 GeV with current up to of 100 μA. In order to achieve the results discussed above, we require the beam time of 17 days in Hall A and 2.5 days in Hall C as it is summarized in Tables 5.

kin. P#	procedure	beam, μA	time, hours	charge Coulomb
P1a	FPP calibration	100	4	1.4
P1b	Beam pol. measurement	1	8	
P1c	BigCal angle change		4	
P1d	RCS data taking	60	40	15
P2a	Beam pol. measurement	8		
P2b	FPP calibration	100	4	1.4
P2c	BigCal angle change		4	
P2d	RSC data taking	100	136	49
P3a	BigCal angle change		4	
P3b	FPP calibration	100	24	9
P3c	BigCal angle change		4	
P3d	RCS data taking	100	224	81
total Hall C			56	17
total Hall A			408	140

Table 5: The beam time request for this experiment.

6 Technical Considerations

6.1 The Cryotarget and Radiator

The standard Hall A/C cryotarget with the machined cells of 15 cm length will be used. This cell type was used with beam current up to 100 μA during recent experiment E99-115. The radiator will be mounted on the cell block as it was done during experiment E99-114.

6.2 The Calorimeter

We plan to use a calorimeter which is under construction for the experiment E01-109 [29]. Figure 20 shows the layout of the detector. It consists of 1750 blocks in 32 columns and 56 rows. The PMT FEU-83-4 will be used for light detection. This Figure also shows configuration of the calorimeter and front end electronics. The stand, which supports the calorimeter and electronics, can be moved into the hall without disassembling, so installation time is needed only for connecting about two thousand 100 m long cables between the detector and DAQ. Such work will require about 70 man-shifts.

The energy resolution for the calorimeter, obtained at the beginning of the experiment E99-114, was 5.5% (for 1 GeV photon energy). It became 10% at the end of the run as result of radiation effects on lead glass transparency (see Fig. 21). Total accumulated beam charge in the experiment E99-114 was 30 Coulomb. In E99-114 the front face of the lead glass was protected by plastic material with effective thickness of 10 g/cm^2. Because it is found that the experiment can be done without veto counters for proposed measurement we plan to use an Al protection sheet of 5 cm thickness to mitigate the radiation damage of the lead glass.

We had developed and tested on the E99-114 calorimeter the technique of curing of the radiation effects. Irradiation by UV light will be done in situ without disassembling of the lead glass stock. However, it is required to remove all PMTs, because large intensity light can damage the photocathode. The whole process of the calorimeter resolution recovery will take about 8 shifts.

6.3 The Proton Spectrometer

The HRS-left will be used in the proposed experiment. The trigger will be done by using S0 and S1 counters. No modification is needed in the double analyzer polarimeter which will be used with two CH_2 analyzers.

6.4 The DAQ for the Calorimeter

The DAQ of the calorimeter, constructed for experiment E04-108, will have almost all components required in the proposed experiment. The coincidence logic between proton and photon arms also will be assembled. In experiment E99-114 the DAQ and HV crates of the calorimeter were located in Hall A near the outer wall at angle of 60° and shielded by 10 inches of the concrete walls from the target and beam dump sides. The trip rate of the

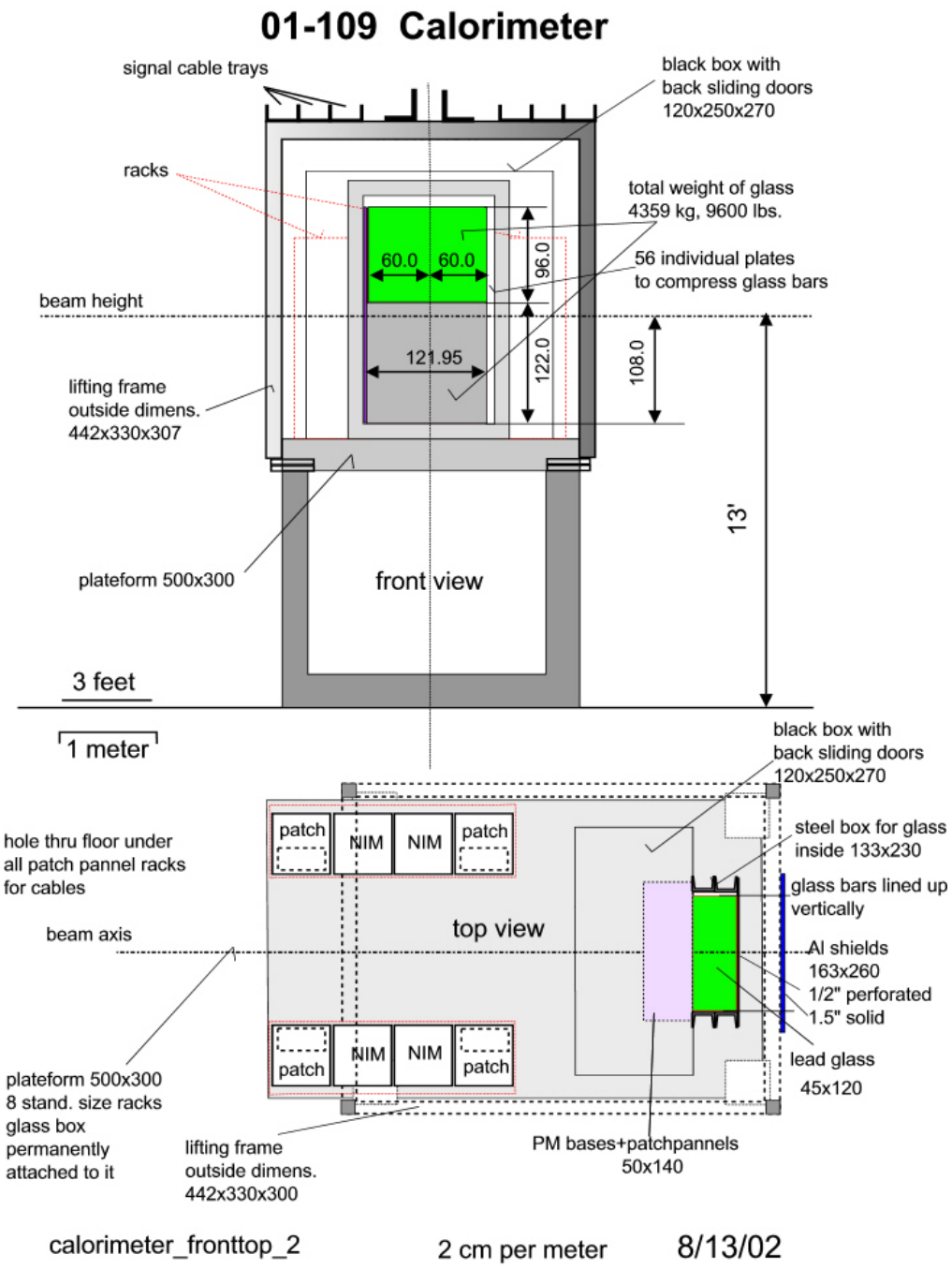

Figure 20: The structure of the BigCal calorimeter and layout of the support stand [29].

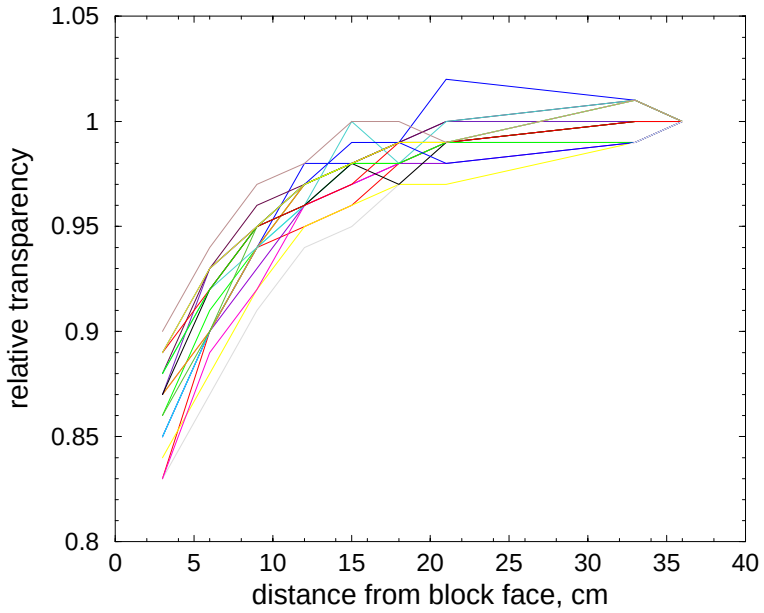

Figure 21: Transparency of lead glass blocks used in E99-114.

CPU was about 1-2 per shift. To mitigate the trip problem we will increase thickness of shielding by an additional 8 inches of concrete or move the DAQ to the 105° position, where the radiation is about 15 times less, according to our calculation and measurements.

7 Conclusions

We request 464 hours of beamtime to measure the longitudinal and transverse components of the polarization transfer in RCS at s= 9 (GeV/c)^2 for θ_p^{cm} = 70, 90, and 110°. This experiment will take place in Hall A for 408 hours and in Hall C for 56 hours, utilizing the polarized electron beam and HRS-left (HMS) spectrometer with the focal plane polarimeter to detect protons, and BigCal calorimeter to detect scattered photons.

Knowledge of the polarization transfer in RCS at these kinematics will allow a rigirous test of the reaction mechanism for exclusive reactions at high t, which is crucial for the understanding of nucleon structure. Futhermore, it will be an extended measurement of the proton axial formfactor in RCS, which is a $1/x$ moment of the polarized parton distribution. We propose to measure polarization transfer K_{LL} in each kinematical point to a statistical accuracy of ± 0.06. Simultaneously the polarization observable P_N will be measured to a statistical accuracy of $\pm(0.10 - 0.15)$, and the polarization observable K_{LT} will be measured to a statistical accuracy of ± 0.05.

References

[1] G. R. Farrar and H. Zhang, *Phys. Rev. Lett.* **41**, (1990) 1721, *Phys. Rev.* **D 65** (1990) 3348.

[2] A. S. Kronfeld and B. Nizic, *Phys. Rev.* **D 44**, 3445 (1991).

[3] M. Vanderhaeghen, P. A. M. Guichon and J. Van de Wiele, *Nucl. Phys.* **A 622**, 144c (1997).

[4] T. Brooks and L. Dixon, *Phys. Rev.* **D 62** 114021 (2000).

[5] A.V. Radyushkin, *Phys. Rev.* **D 58**, 114008 (1998).

[6] M. Diehl, T. Feldmann, R. Jakob, P. Kroll, *Eur. Phys. J.* **C 8**, 409 (1999).

[7] H. W. Huang, P. Kroll, T. Morii, *Eur. Phys. J.* **C 23**, 301 (2002).

[8] F. Cano and J. M. Laget, *Phys. Rev.* **D 65**, 074022 (2002)

[9] C. Hyde-Wright, A. Nathan, and B. Wojtsekhowski, spokespersons, JLab experiment E99-114.

[10] D. J. Hamilton, V. H. Mamyan *et al.*, *Phys. Rev. Lett.* **94**, 242001 (2005).

[11] M. Diehl *et al.*, *Phys. Rev.* **D 67**, 037502 (2003).

[12] G. A. Miller, *Phys. Rev.* **C 69**, 052201(R) (2004).

[13] F. Cano and J. M. Laget, *Phys. Lett.* **B 551**, 317 (2003).

[14] M. A. Shupe *et al.*, *Phys. Rev.* **D 19**, 1921 (1979).

[15] S. J. Brodsky and G. P. Lepage in *Perturbative Quantum Chromodynamics*, edited by A. Mueller (World Scientific, Singapore, 1989).

[16] S. J. Brodsky and G. Farrar, *Phys. Rev. Lett.* **31**, 1953 (1973).

[17] V. Matveev *et al.*, *Nuovo Cimento Lett.* **7**, 719 (1973).

[18] S. J. Brodsky and G. P. Lepage, *Phys. Rev.* **D 22**, 2157 (1980).

[19] M. Jones *et al.*, *Phys. Rev. Lett.* **84**, 1398 (2000).

[20] O. Gayou *et al.*, *Phys. Rev. Lett.* **88**, 092301 (2002).

[21] K. Wijesooriya *et al.*, *Phys. Rev. C***66**, 034614 (2002).

[22] M. Diehl *Phys. Rept.* **388**, 41-277 (2003).

[23] X. Ji, *Phys. Rev.* **D 55**, 7114 (1997), *Phys. Rev. Lett.* **78**, 610 (1997).

[24] A.V. Radyushkin, *Phys. Lett.* **B 380**, 417 (1996), *Phys. Rev.* **D 56**, 5524 (1997).

[25] E. Lomon, *Phys. Rev.* **C 66**, 045501 (2002).

[26] R. L. Anderson *et al.*, *Phys. Rev.* **D 14**, 679 (1976).

[27] M. Battaglieri *et al.*, *Phys. Rev. Lett.* **87**, 172002 (2001).

[28] T. H. Bauer, *et al.*, *Rev. Mod. Phys.* **50**, 261 (1978).

[29] C. Perdrisat *et al.*, JLab experiment E01-109, 2001.

[30] B. Bonin *et al.*, *Nucl. Instr. Meth.* **A 288**, 379 (1991).

[31] I. M. Sitnik *et al.*, private communication, 2002.

[32] A. I. Akhiezer and M. P. Rekalo, *Sov. J. Nucl. Phys.* **3**, 277 (1974).

[33] R. Arnold, C. Carlson and F. Gross, *Phys. Rev.* **C 23**, 363 (1981).

[34] C. Perdrisat and L. Pentchev, private communtication, 2002.

[35] D. Day and B. Wojtsekhowski, spokespersons, JLab experiment E05-101.

[36] V. L. Chernyak and A. R. Zhitnitsky, *Phys. Rep.* **112**, 173 (1984).

[37] V. L. Chernyak, A. A. Oglobin, and A. R. Zhitnitsky, *Z. Phys.* **C 42**, 569 (1989).

[38] I. D. King and C. T. Sachrajda, *Nucl. Phys.* **A 598**, 785 (1987).